Designed Nanocage Displaying Ligand-Specific Peptide Bunches for High Affinity and Biological Activity

Jae Og Jeon,[†,∥] Soyoun Kim,[†,∥] Eunsu Choi,[‡] Kihyuk Shin,[‡] Kiweon Cha,[§] In-Seop So,[†] Sun-Ji Kim,[†] Eunsung Jun,[†,⊥] Dohee Kim,[†] Hyung Jun Ahn,[⊥] Byung-Heon Lee,[†] Seung-Hyo Lee,[‡,*] and In-San Kim[†,⊥,*]

[†]Department of Biochemistry and Cell Biology, Cell and Matrix Research Institute, School of Medicine, Kyungpook National University, Daegu 700-422, Republic of Korea, [‡]Graduate School of Medical Science and Engineering, Biomedical Research Center, KAIST Institute for the BioCentury, Korea Advanced Institute of Science and Technology, Daejeon 305-701, Republic of Korea, [§]Division of High-Risk Pathogen Research, Korea National Institute of Health (KNIH), Korea Centers for Disease Control & Prevention (KCDC), Osong, Chungbuk 363-951, Republic of Korea, and [⊥]Biomedical Research Institute, Korea Institute of Science and Technology, Seoul 136-791, Republic of Korea. [∥]J. O. Jeon and S. Kim contributed equally to this work.

ABSTRACT Protein-cage nanoparticles are promising multifunctional platforms for targeted delivery of imaging and therapeutic agents owing to their biocompatibility, biodegradability, and low toxicity. The major advantage of protein-cage nanoparticles is the ability to decorate their surfaces with multiple functionalities through genetic and chemical modification to achieve desired properties for therapeutic and/or diagnostic purposes. Specific peptides identified by phage display can be genetically fused onto the surface of cage proteins to promote the association of nanoparticles with a particular cell type or tissue. Upon symmetrical assembly of the cage, peptides are clustered on the surface of the cage protein in bunches. The resulting PBNC (peptide bunches on nanocage) offers the potential of synergistically increasing the avidity of the peptide ligands, thereby enhancing their blocking ability for therapeutic purposes. Here, we demonstrated a proof-of-principle of PBNCs, fusing the interleukin-4 receptor (IL-4R)-targeting peptide, AP-1, identified previously by phage display, with ferritin-L-chain (FTL), which undergoes 24-subunit assembly to form highly stable AP-1-containing nanocage proteins (AP1-PBNCs). AP1-PBNCs bound specifically to the IL-4R-expressing cell line, A549, and their binding and internalization were specifically blocked by anti-IL-4R antibody. AP1-PBNCs exhibited dramatically enhanced binding avidity to IL-4R compared with AP-1 peptide, measured by surface plasmon resonance spectroscopy. Furthermore, treatment with AP1-PBNCs in a murine model of experimental asthma diminished airway hyper-responsiveness and eosinophilic airway inflammation along with decreased mucus hyperproduction. These findings hold great promise for the application of various PBNCs with ligand-specific peptides in therapeutics for different diseases, such as cancer.

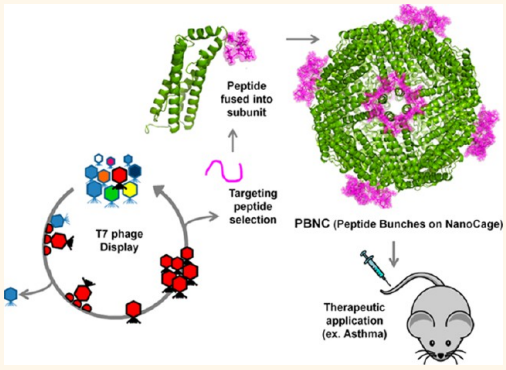

KEYWORDS: protein cage · nanoparticles · AP-1 peptide · IL-4 receptor · asthma

Nanoparticle-based technology has seen significant progress in recent decades and has been extensively studied for potential biomedical applications, including controlled drug/gene delivery, tissue engineering, and molecular imaging.[1−4] In particular, therapies using nanoparticles have been widely applied for the treatment of various types of diseases including cancer,[5] diabetes,[6] allergy,[7] infection,[8] and inflammation.[9] Nanoparticles, whose sizes are on the same order as those of proteins, are rapidly absorbed and pass through biological barriers in the body; moreover, their large surface areas allow for the presentation of large numbers of functional groups, such as ligands.[10,11]

Protein-based nanoparticles, comprising naturally self-assembled protein subunits of the same proteins or a combination of proteins, offer advantages of biocompatibility, biodegradability, and low toxicity compared with synthetic polymers.[12,13] In addition to these inherent advantages, protein-cage nanoparticles provide additional advantages. First, because of their unique shape with symmetric architectures, additional moieties can be mounted on distinct regions of protein nanocages through genetic modification. Rationally designed multifunctionality, such as active targeting or

* Address correspondence to (I.-S. Kim) iskim@knu.ac.kr; (S.-H. Lee) sl131345@kaist.ac.kr.

Received for review June 24, 2013 and accepted August 8, 2013.

Published online August 08, 2013
10.1021/nn403184u

image-contrast enhancement, is one expected characteristic of nanoparticles currently under development. Second, the applicability of genetic modifications, which are relatively simple and inexpensive, is critically beneficial from the standpoint of pharmaceutical development because the cost/benefit ratio must be considered for translation of nanoparticle drugs into the clinical domain.[14,15]

Here, we describe a protein-cage nanoparticle loaded with receptor-targeting peptides that is genetically encodable with no synthetic components. Nanocage proteins are designed such that these peptides are symmetrically clustered on the surface in a form that we have termed peptide bunches on nanocage (PBNC)—a structure that is predicted to increase the avidity of the peptide ligands and thus enhance their blocking ability in therapeutic applications.

Because peptide-based recognition systems are capable of overcoming problems associated with antibodies, such as high cost, fast clearing due to opsonization, and difficulties associated with modification, we utilized small peptides from phage-display libraries.[16] Phage display is a powerful method for identifying and developing peptide drugs, but peptides consisting of 6−10 amino acids often have the drawbacks of weak affinity and short half-life.[17] Multivalency and multispecificity of PBNCs can help to overcome the weak affinity, prolong the half-life, and, in some cases, promote endocytic uptake. We employed ferritin, which is composed of 24 subunits, as a protein cage. The subunits assemble into hollow, 12-nm-diameter cages that present three distinct interfaces: interior, exterior, and self-interacting surfaces.[18] The uniform size and symmetric architecture allows for the loading of an even number of targeting peptides into the expected regions and designing functionality into the designated interfaces. Ferritin possesses many useful properties, such as high solubility, stability, abundance in blood, and low toxicity, which have motivated studies on its use as a prototype of protein-cage nanoplatforms in the development of diverse applications.[19,20]

As proof-of-principle of PBNCs, we focused on asthma, a complex immune-related disease characterized by chronic inflammation of the airways, airway hyper-responsiveness (AHR), and reversible airflow obstruction.[21,22] To date, curative therapeutics for asthma have not been developed, and only symptom relievers and controllers, including inhaled corticosteroids, β2 agonists, and histamine and leukotriene inhibitors, are currently available.[23−25] Asthma is one of the most common chronic inflammatory diseases in the world, and many of its features are thought to reflect consequences of immune responses by allergen-specific T-helper type 2 (Th2) cells. Th2 cells act on epithelial and smooth muscle cells of the airway to induce mucus hyperproduction and AHR through secretion of interleukin (IL)-4 and IL-13.[26,27] In addition, IL-5 secreted by Th2 cells mediates recruitment of eosinophils, leading to the manifestation of tissue eosinophilia. A key pathway that regulates chronic inflammation and tissue remodeling in allergic asthma is ligation of IL-4 and/or IL-13 to their receptor complexes and activation of signaling events initiated by IL-4 receptor α (IL-4Rα).[28] This pathway regulates various aspects of Th2 cell-mediated responses, including induction of immunoglobulin E (IgE) isotype switching, modulation of lymphocyte and antigen-presenting cell functions, and tissue inflammation and remodeling. Targeted disruption of the IL-4Rα subunit in mice abrogates the IgE response, which is consistent with the crucial function of L-4Rα in controlling the allergic response.[29] Thus, biological compounds that target IL-4Rα may provide a potent therapeutic modality for patients with asthma.

With this rationale in mind, we describe the construction of AP1-PBNCs and their utility in blocking IL-4Rα in an animal model of asthma. The previously identified AP-1 peptide was shown to bind selectively to the IL-4Rα subunit and block IL-4R-mediated signaling.[30] Here, we show that AP1-PBNCs are easily expressed in high yields in *Escherichia coli* and assemble as 24-subunit structures that bind IL-4Rα with high affinity. We further demonstrate that AP1-PBNCs attenuate the severity of murine experimental asthma by selectively suppressing AHR, bronchoalveolar lavage (BAL) eosinophilia, and mucus hypersecretion. Our data suggest possible therapeutic applications of various PBNCs with peptides targeting different diseases, such as cancer.

RESULTS AND DISCUSSION

Ferritin, which is composed of 24 subunits, forms a cage architecture with inner and outer diameters of 8 and 12 nm, respectively.[18] Each subunit consists of four long helical bundles (helices A−D) and a tilted short α-helix (helix E) connected by a short loop (Figure 1b). The human ferritin light (FTL) chains, which lack the ability to catalyze oxidation of Fe^{2+} (II) to Fe^{3+} (III), were utilized for PBNC construction. AP-1 peptides, identified by phage display, were genetically combined into the exposed loop region (^{155}LGGPE^{159}) between helices D and E (Figure 1a). The peptides in the phage library contain cysteine residues on both sides; when oxidized, they help the peptide adopt a loop conformation. We inserted two amino acid sequences of AP-1, with or without cysteine (RKRLDRN, CRKRLDRNC), into two different positions (before positions 157 and 158) to determine the best functional orientation of peptides; we termed these constructs ^{157}AP1-PBNC, ^{157}cysAP1-PBNC, ^{158}AP1-PBNC, and ^{158}cysAP1-PBNC (Figure 1a). We also introduced two restriction enzyme sites (*Bam*HI and *Apa*I) for convenient insertion of peptides. The AP1-fused FTL subunit was built by

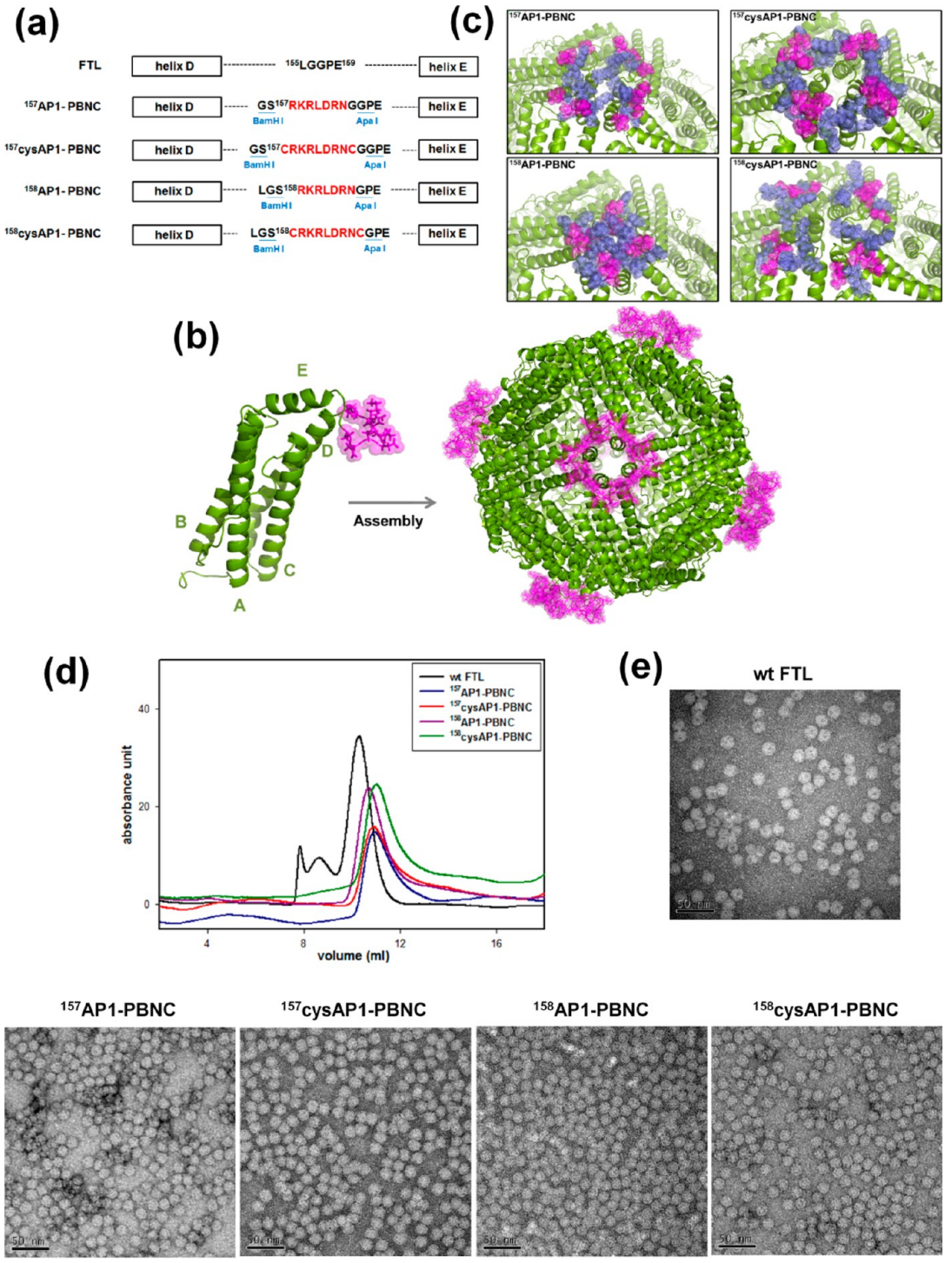

Figure 1. (a) Schematic diagram of the AP1-PBNCs. Two amino acid sequences of the AP-1 peptide, with or without cysteine (RKRLDRN, CRKRLDRNC, highlighted in red), were inserted into two different positions (before positions 157 and 158) between helices D and E. *Bam*HI and *Apa*I enzyme sites (blue color) were introduced for convenient insertion of peptides. (b) 3D model of the AP-1 peptide inserted ferritin subunit and assembled AP1-PBNCs. The AP-1 peptide (magenta) inserted ferritin subunit (green) was calculated based on the wt ferritin crystal structure (PDB 2FG4). The calculated 24 subunits were assembled into AP1-PBNC by computer simulation based on the wild-type ferritin cage structure (PDB 3A68) (c) Enlarged four types of AP-1 peptide insertion on the 4-fold axis; basic residues of the AP-1 peptide are highlighted in light blue. (d) Size exclusion elution profiles of wt FTL and AP1-PBNCs. (e) Transmission electron micrographic image of uracil acetate stained wt FTL and AP1-PBNCs.

homologous modeling with Modellar v9.1 using the crystal structure of wild-type (wt) human ferritin (2FG4) as a template and assembled into AP1-PBNC by computer simulation based on the wt ferritin cage structure (PDB 3A68) shown in Figure 1b. The model showed that four copies of AP-1 peptides were

clustered onto the 4-fold symmetry-assembling regions, forming peptide bunches, and six bunches were displayed on the nanocage surface. Interestingly, the four different AP1-PBNCs showed slightly different patterns of peptide bunching; notably, the peptide bunches of cysAP1-fused AP1-PBNCs (^{157}cysAP1-PBNC and ^{158}cysAP1-PBNC) formed wider bunches than those of ^{157}AP1-PBNC and ^{158}AP1-PBNC (Figure 1c).

The four different AP1-PBNCs were characterized by size-exclusion chromatography (SEC) and transmission electron microscopy (TEM) and compared with wt ferritin cage proteins (wt FTL) lacking displayed peptides. All AP1-PBNCs eluted at a position similar to that of wt FTL in SEC, suggesting that AP-1 peptide modification did not hamper formation of authentic cage architectures (Figure 1d). TEM images also confirmed that AP1-PBNCs formed an intact, cage architecture with a uniform size distribution (Figure 1e). These results indicate that the four different types of AP1-PBNCs form intact, cage nanoparticle architectures without significant discrepancies.

To test the binding of AP1-PBNCs to IL-4R, we first employed fluorescence-activated cell sorting (FACS) analysis to compare their capacity to bind A549 cells expressing IL-4R on the cell surface. The binding of AP1-PBNCs to A549 cells was significantly enhanced compared with that of wt FTL (Figure 2a). Preincubation of A549 cells with anti-IL-4R antibody disrupted binding, indicating that AP1-PBNCs specifically target IL-4R (Figure 2a). In addition, the binding of AP1-PBNC to A549 cells was decreased by the knockdown of the IL-4R expression (Figure S1). We also examined specific targeting of AP1-PBNCs to the A549 cell membrane with confocal microscopy, which showed that AP1-PBNCs bound to A549 cells, whereas wt FTL did not (Figure 2b). After incubation of A549 cells with AP1-PBNCs at 37 °C for 1 h, AP1-PBNCs were translocated into the cytosol *via* receptor-mediated endocytosis, whereas wt FTL was not (Figure 2c). The IL-4R-specific endocytosis of AP1-PBNCs could be an important advantage of AP1-PBNCs for protein-based drug delivery because most native proteins are barely taken up by cells. Taken together, these results suggest that the presence of AP1-PBNCs is responsible for nanoparticle binding to IL-4R-expressing cells and cellular uptake through IL-4R-mediated endocytosis; thus, up-regulation of IL-4R expression would play a critical role in cytoplasmic uptake of AP1-PBNCs. Accordingly, because AP1-PBNCs would be selectively transported into IL-4R-expressing cells, they could be used not only for molecular targeting but also for the selective delivery of drugs.

Multivalent display of targeting moieties on the surface of nanoparticles increases binding strength through increased target binding avidity without changing the affinity for the individual target sites.[31] We use "binding avidity" rather than "binding affinity" to describe the overall binding strength of AP1-PBNCs, since the binding affinity of individual sites could be heterogeneous, whereas the avidity, defined as the ability to form a stable complex with a target, depends on intrinsic affinity and is enhanced with increasing numbers of binding sites.[32] We expected that the multivalent conjugation of AP-1 on the surface of FTL nanoparticles would enhance the binding avidity to the designated target, IL-4R. To investigate the binding avidity of AP1-PBNCs to IL-4Rα, we immobilized a component of the extracellular region of the IL-4R, applied a series of different concentrations of AP1-PBNCs, and examined binding kinetics using surface plasmon resonance (SPR) analysis. Binding responses gradually increased upon addition of increasing concentrations of AP1-PBNCs (Figure 3a); in contrast, wt FTL did not bind to IL-4Rα (Figure S2). The values of the overall dissociation constants, K_D (multivalent, K_D-(multivalent)), for AP1-PBNCs were calculated (Figure S3) and compared with those of free AP-1 peptide as well as IL-4, the natural ligand for IL-4R (Table 1). As expected, the binding avidity of the multivalent AP1-PBNCs was markedly increased compared to that of free AP-1 peptide (Table 1). To evaluate the enhanced binding strength of AP1-PBNCs, we calculated the multivalent enhancement ratio (β), the ratio of the monovalent K_D (free AP-1 peptide) to the multivalent K_D (AP1-PBNCs). The avidity of the multivalent AP1-PBNCs was increased by about 10^6 fold (Table 1). This increase in binding avidity of AP1-PBNCs was largely due to the exponential decrease in K_D, which is a typical phenomenon for multivalent binding.[32] Indeed, 24 copies of AP-1 peptides were incorporated and displayed on the surface of one nanoparticle, and some were able to interact with IL-4R simultaneously, thereby enhancing binding avidity. Cysteine-containing, AP1-conjugated PBNCs (^{157}cysAP1-PBNC and ^{158}cysAP1-PBNC) exhibited superior binding ability compared with AP1-conjugated PBNCs (^{157}AP1-PBNC and ^{158}AP1-PBNC), as evidenced by their significantly higher binding responses (Figure 3b). The wide distribution of positive charges of AP-1 peptide bunches in ^{157}cysAP1-PBNC and ^{158}cysAP1-PBNC may promote higher binding affinity through formation of a stable complex. Because ^{157}cysAP1-PBNC exhibited the highest binding response (RU value), we selected this PBNC for subsequent *in vivo* experiments.

IL-4, IL-13, and signal transducer and activator of transcription (STAT) 6 are key components in the development of airway inflammation, mucus hyperproduction, and AHR in asthma.[22] After ligation of either IL-4 or IL-13, IL-4R is phosphorylated and activates Janus kinases (Jaks), which act as docking sites for STAT6.[33] Recruited STAT6 is phosphorylated, then dimerizes and is translocated into the nucleus, where it binds the promoters of IL-4- and/or IL-13-responsive genes associated with Th2 cell differentiation, airway inflammation, AHR, and mucus production. A previous

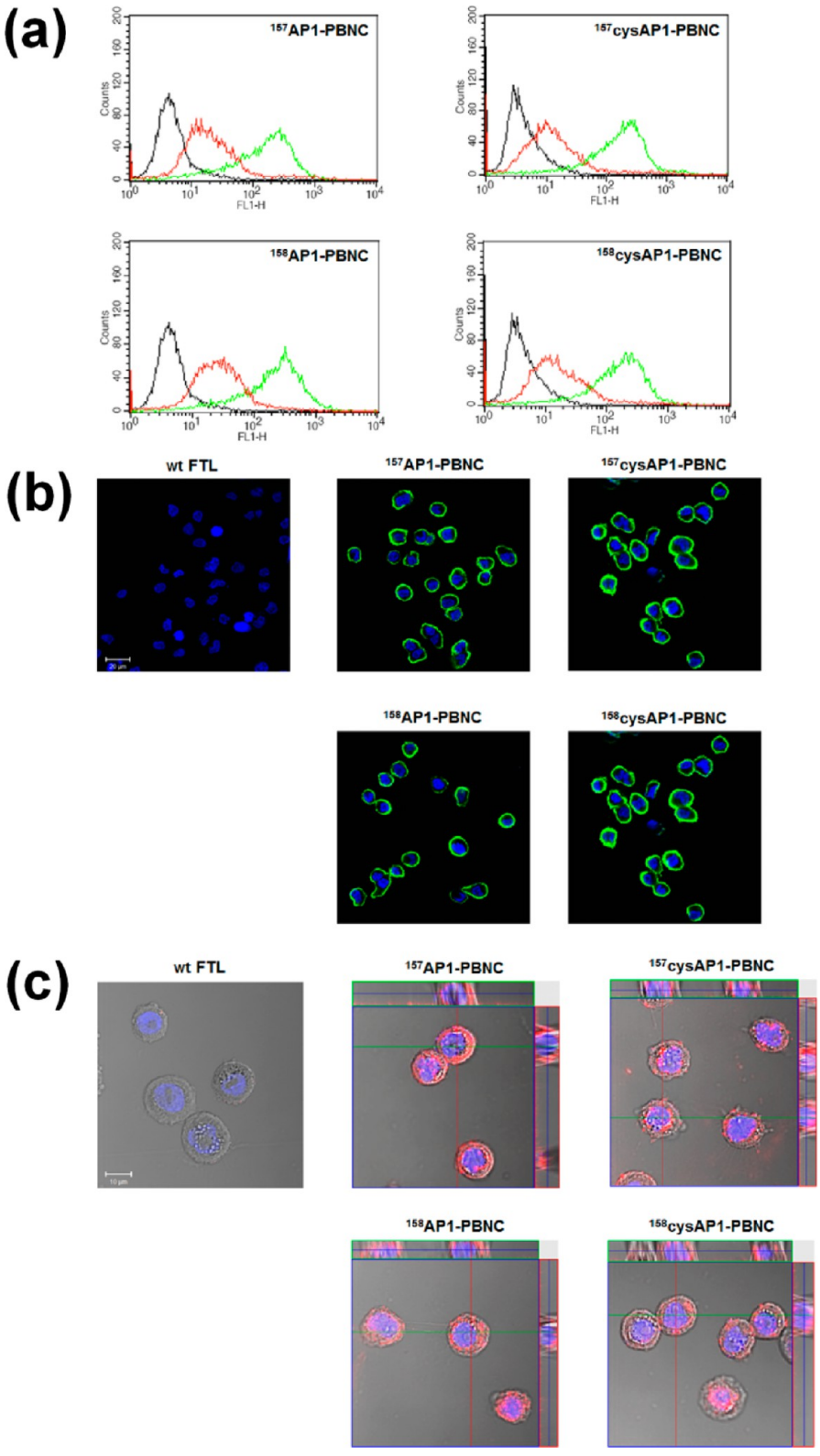

Figure 2. (a) FACS analysis of A549 cells incubated with or without anti-IL-4R antibody prior to incubation with wt FTL and AP1-PBNCs. The black and green lines indicate cells incubated with wt FTL and AP1-PBNCs, respectively. The red line indicates cells preincubated with anti-IL-4R antibody. (b) Fluorescence images of wt FTL and AP1-PBNCs after 20 min incubation at 4 °C (cell binding) or (c) 1 h incubation at 37 °C (cellular uptake). This has been performed by Z stack confocal fluorescence microscopy images; nuclei are stained blue.

study has demonstrated that the development of allergic lung inflammation requires activation of STAT6 not only in T cells but also in the parenchymal cells of the lung.[34] Numerous studies strongly support the idea

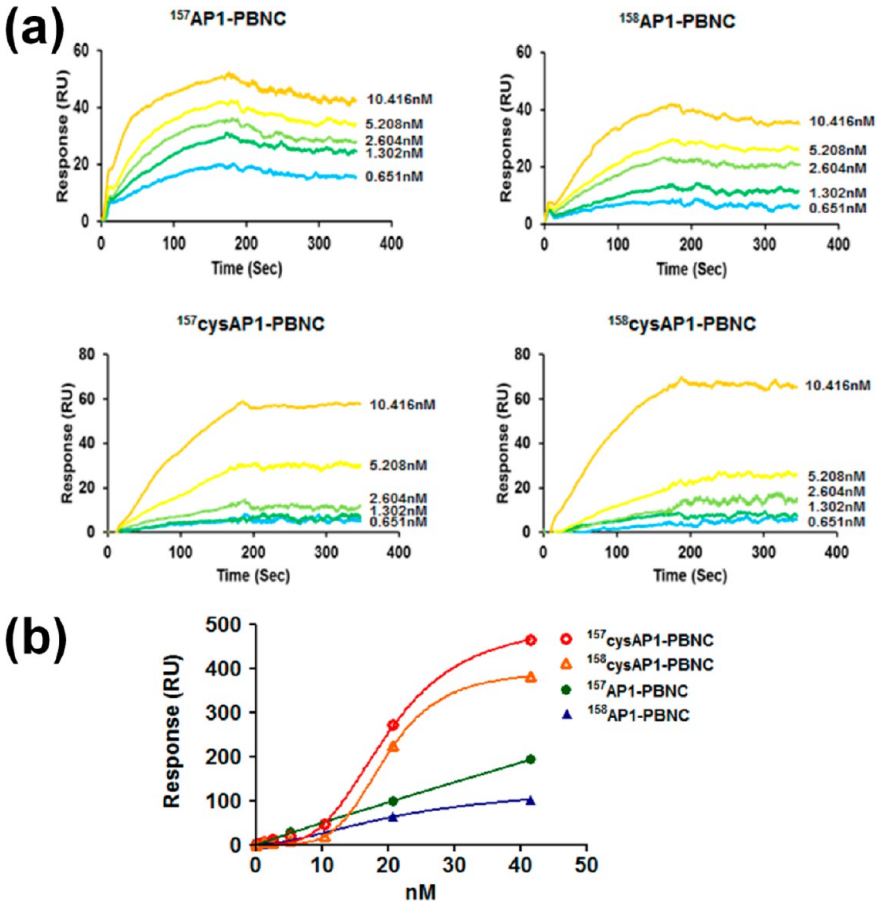

Figure 3. Surface plasmon resonance studies for the binding kinetics of IL-4Rα and AP1-PBNCs. (a) The concentrations of AP1-PBNCs injected are indicated. (b) Plots of RU values of AP1-PBNCs *versus* different injection concentrations.

TABLE 1. Quantified Binding Constants of the AP1-PBNCs with IL-4Rα Measured by SPR

ligand	K_D (M)[a]	β[b]
IL-4[39]	3.82×10^{-10}	
AP-1 peptide	$5.54(\pm 0.3) \times 10^{-3}$	
^{157}AP1-PBNC	$3.9(\pm 1.9) \times 10^{-9}$	1.4×10^{6}
^{157}cysAP1-PBNC	$2.3(\pm 0.9) \times 10^{-9}$	2.4×10^{6}
^{158}AP1-PBNC	$3.2(\pm 1.5) \times 10^{-9}$	1.7×10^{6}
^{158}cysAP1-PBNC	$2.9(\pm 1.4) \times 10^{-9}$	1.9×10^{6}

[a] Obtained by averaging at least three independent runs of SPR measurements. [b] Multivalency parameter $\beta = K_D(\text{free})/K_D(\text{multivalent})$.

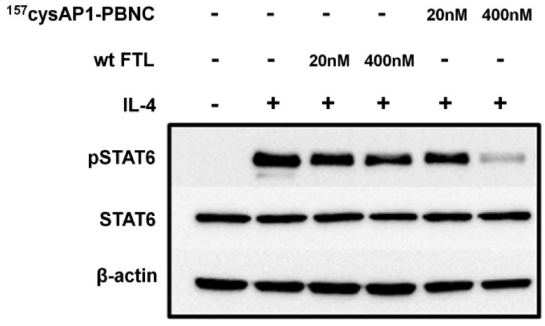

Figure 4. Inhibition of IL-4R signaling pathway upon binding of ^{157}cysAP1-PBNC to IL-4Rα. The phosphorylation of STAT6 by IL-4 was measured with Western blot analysis with addition of ^{157}cysAP1-PBNC or wt FTL.

that STAT6 plays a central role in the pathogenesis of allergic asthma.[34−37] To test the blockade of IL-4R-mediated signaling by AP1-PBNCs (^{157}cysAP1-PBNC) *in vitro*, we examined the level of STAT6 phosphorylation by Western blot analysis. The degree of STAT6 phosphorylation was significantly diminished by treatment with ^{157}cysAP1-PBNC (200 nM), which presumably blocked IL-4R-mediated signaling (Figure 4). The excess amount of IL-4 competitively inhibited the binding of ^{157}cys AP1-PBNC to A549 cells, suggesting that AP1-PBNCs could block IL-4-mediated signaling (Figure S4). This result indicates that blocking IL-4R signaling with ^{157}cysAP1-PBNC could be a good therapeutic strategy for IL-4-dependent diseases, including allergic asthma.

To test ^{157}cysAP1-PBNC as a possible asthma therapy, we investigated the murine experimental asthma phenotype induced by *Aspergillus* protease and chicken egg ovalbumin (APO) allergen, which is characterized by increased AHR, enhanced numbers of inflammatory cells, and mucus production in BAL fluid. Compared with the saline-challenged group, groups

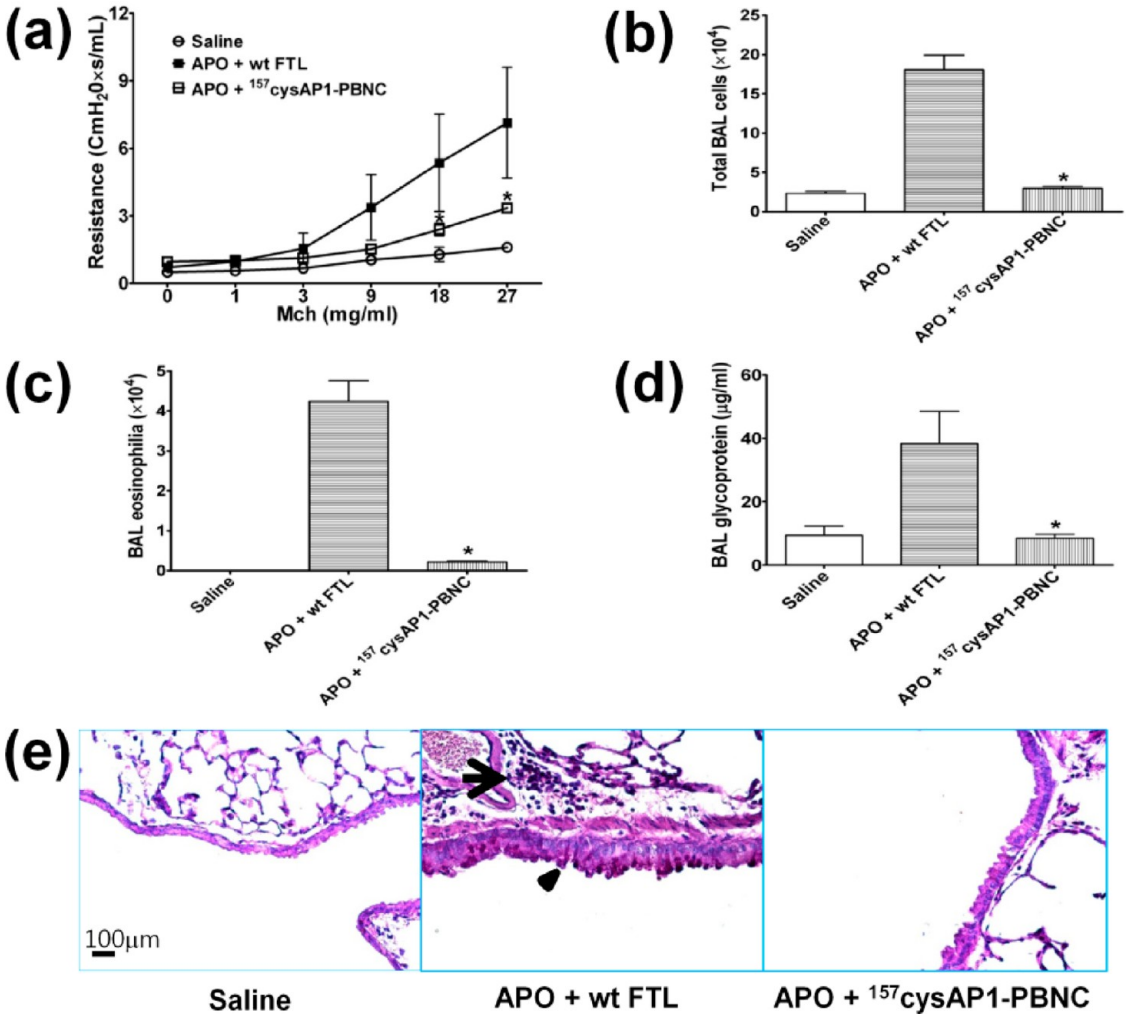

Figure 5. ^{157}cysAP1-PBNC-attenuated phenotypes of murine experimental asthma. Experimental asthma was induced with *A. oryzae* protease mixed with OVA (APO) allergen along with wt FTL or ^{157}cysAP1-PBNC. Saline means negative control without allergen challenge. AHR with a FlexiVent system (a), total BAL cell counting (b), and BAL eosinophilia (c) were determined. (d) Secreted airway glycoprotein in BAL was quantified by modified ELISA. (e) The periodic acid Schiff (PAS) stained sections of the lungs showed increased inflammatory cells and goblet cell metaplasia in APO- and wt FTL-treated group (arrowhead: mucin-positive goblet cell, arrow: inflammatory cell, original magnification of 400×). Data are presented as mean ± SEM, *$p < 0.05$ *versus* APO + wt FTL treatment. Data are representative of three independent experiments ($n = 3$ per group).

challenged with APO with wt FTL showed increased AHR. However, APO-challenged animals treated with ^{157}cysAP1-PBNC showed significantly reduced airway resistance compared with that of animals in the APO and wt FTL group (Figure 5a). In addition, the number of inflammatory cells, especially eosinophils, in BAL fluid was significantly diminished in the group treated with ^{157}cysAP1-PBNC compared to the group administered wt FTL (Figure 5b and c). Furthermore, secreted glycoprotein in BAL fluid, which was clearly enhanced in APO- and wt FTL-treated groups, was decreased with ^{157}cysAP1-PBNC treatment (Figure 5d). Lastly, the APO-challenged group treated with ^{157}cysAP1-PBNC showed decreased numbers of peribronchial inflammatory cells and mucus-producing goblet cells (Figure 5e). Collectively, these results indicate that administration of ^{157}cysAP1-PBNC diminished the symptoms of murine experimental asthma, suggesting an inhibitory effect on allergic asthma. In order to test the potential immunogenicity of AP1-PBNCs, we pretreated AP1-PBNCs with human/mouse monocytic cell lines and measured the amount of secreted cytokines (Figure S5). The representative proinflammatory cytokines (IL-6 and IL-12) were not significantly enhanced by treatment of AP1-PBNCs with the THP-1 cells compared to wild-type ferritin and mock treatment, whereas LPS significantly increased IL-6 production. Largely similar results were obtained in the RAW 264.7 cells. These data suggest that AP1-PBNCs might not be immunogenic but need further *in vivo* studies for clinical application. A number of biological compounds are currently being developed for the treatment of asthma, including soluble IL-4R compounds,[38] an IL-4 variant,[39] and anti-IL-13 monoclonal antibody;[40] however, further studies are needed to evaluate their efficacy as well as long-term safety. Here, we provide

a novel approach for therapeutic intervention against allergic asthma using ferritin nanoparticles.

CONCLUSIONS

We have demonstrated that ferritin cage nanoparticles can be engineered by genetic incorporation of targeting peptides for use as a cell-specific targeting agent. Upon assembly of the cage architecture, IL-4R-targeting AP-1 peptides are displayed in bunches on the nanocage surface (AP1-PBNCs), producing high binding avidity and selectivity suitable for therapeutic applications. *In vitro*, AP1-PBNCs specifically bind to IL-4Rα, a major component of IL-4R, resulting in significantly improved targeting capacity. *In vivo*, administration of AP1-PBNCs, specifically ^{157}cysAP1-PBNC, diminished the symptoms of allergic asthma, including AHR, airway eosinophilia, and mucus hyperproduction, in murine experimental asthma. These results carry significant implications for protein nanocage platform technology. First, this approach employs targeting of a human cage-like, protein-based nanoparticle for an immune-related disease. Notably, ferritin cage proteins decorated with peptide bunches showed therapeutic efficiency in an animal model of asthma. Second, and perhaps more importantly, these findings suggest a possible therapeutic application of various PBNCs with peptides targeting different diseases, such as cancer.

METHODS

Construction of AP-1 Peptide Conjugated Ferritin (AP1-PBNCs). The recombinant plasmid for the expression of wt FTL proteins was described previously.[41] The AP-1 peptides (RKRLDRN and CRKRLDRNC) were incorporated at the 157 and 158 positions of wt FTL. *Bam*HI and *Apa*I restriction sites were introduced into wt FTL for subsequent incorporation of the AP-1 peptide sequences by using PCR-mediated site-directed mutagenesis. The primers encoding AP-1 peptides were mixed at a 1:1 molar ratio, annealed at 95 °C, and inserted into the introduced *Bam*HI and *Apa*I site of the plasmid. The insertion of the AP-1 peptide sequences resulted in the change of the original amino acid sequence of wt FTL from ^{155}LGGPE to ^{155}GSRKRLDRNGGPE (^{157}AP1-PBNC), ^{155}GSCRKRLDRNCGGPE (^{157}cysAP1-PBNC), ^{155}LGSRKRLDRNGPE (^{158}AP1-PBNC), and ^{155}LGSCRKRLDRNCGPE (^{158}cysAP1-PBNC) (Figure 1a).

Protein Expression and Purification. The proteins were overexpressed in *E. coli* BL21 (DE3) cells. Cells were grown at 37 °C to an OD_{600} of 0.5 in LB medium containing 50 μg/mL kanamycin, and protein expression was induced by 1 mM IPTG at 20 °C for 18 h. After induction, cells were harvested by centrifugation, and the pellets were suspended in lysis buffer (20 mM Tris-HCl pH 8.0, 100 mM NaCl, 1 mM EDTA, 1% Triton X-100, 1 mM PMSF, 0.5 mM DTT) and homogenized with an ultrasonic processor. The inclusion bodies from cell lysates were solubilized by incubating in binding buffer (20 mM Tris-HCl pH 8.0, 500 mM NaCl, 5 mM imidazole) containing 8 M urea at room temperature for 1 h. Afterward, the denatured protein was loaded onto a nickel ion chelate affinity column and refolded with a gradient of 8−0 M urea. The renatured protein was eluted with elution buffer (20 mM Tris-HCl pH 8.0, 150 mM NaCl, 180 mM histidine).

Characterization of AP1-PBNCs. After purification, each protein was analyzed by SEC (Superdex 200 10/300 GL column). Oligomeric states were judged from the elution volume compared with molecular weight standard. Protein elution profiles in SEC were monitored by measuring absorbance at 280 nm. TEM pictures were recorded using an FEI Tecnai (the Korea Basic Science Institute, KBSI).

Cell-Binding and -Uptake Studies. Human lung cancer cell line A549 was cultured in RPMI 1640 supplemented with 10% fetal bovine serum, 100 units/mL penicillin, and 100 μg/mL streptomycin. To perform cell binding analysis, 2×10^5 cells in suspension were incubated with 1% bovine serum albumin at 37 °C for 30 min for blocking and incubated with 400 nM wt FTL or AP1-PBNCs at 4 °C for 20 min. The binding specificity of AP1-PBNCs was also measured in blocking experiments in which A549 cells were preincubated with antibody to human IL-4R (1:1000 dilution, MAB230, R&D Systems, Abingdon, UK) at 4 °C for 1 h. Cells were then incubated with human ferritin light chain antibody (1:400 dilution, SC-14420, Santa Cruz Biotechnology Inc., Dallas, TX, USA) and detected with Alexafluor 488-conjugated donkey anti-goat IgG (H+L) antibody (Invitrogen, Molecular Probes, Eugene, OR, USA). The cells were resuspended in PBS and analyzed with FACS Calibur cytometry (BD Biosciences, San Jose, CA, USA). For confocal microscopic analysis, cells were attached in eight-chamber culture slides by centrifugation, the nuclei were stained with DAPI, and slides were mounted and analyzed (Carl Zeiss, Oberkochen, Germany).

For cellular uptake analysis, A549 cells were seeded in eight-chamber culture slides at a density of 1×10^4 cells/chamber and allowed to adhere to the slides overnight. Cells were incubated with 400 nM wt FTL or AP1-PBNCs at 37 °C for 1 h and then treated with cold methanol at −20 °C for 20 min for membrane permeability. Cells were detected with anti-His probe (H-15) AlexaFluor 647 antibody (1:40 dilution, Invitrogen) at 4 °C overnight. To observe the distribution of nanoparticles in cytoplasm, we performed *z*-sectional imaging analysis by confocal microscopy (Carl Zeiss).

Surface Plasmon Resonance Analysis. Interactions of AP1-PBNCs with IL-4R were analyzed at 25 °C using a surface plasmon resonance instrument (SR7500 DC, Reichert Inc., NY, USA). IL-4Rα was expressed and purified in Sf21 cells. After purification, IL-4Rα was immobilized by activating the carboxymethyl group on dextran-coated chips through a reaction with a mixture of *N*-(3-dimethylaminopropyl)-*N*′-ethylcarbodiimide hydrochloride and *N*-hydroxysuccinimide (Sigma-Aldrich, St. Louis, MO, USA). Different concentrations of AP1-PBNCs (0.65 to 41.6 nM) in binding buffer (20 mM Tris, 150 mM NaCl, 180 mM histidine, 62.5 μg/mL BSA, 0.005% Tween 20) were allowed to flow over surfaces containing immobilized IL-4Rα (1500 ± 500 RU) for 7 min at a rate of 25 μL/min. The sensor surface was regenerated after each association and dissociation cycle by injecting 2 M NaCl for 1 min. The interaction was analyzed using Scrubber 2.0 (BioLogic Software, Australia, and KaleidaGraph Software, Australia).

STAT6 Phosphorylation. A549 cells were plated at 1.2×10^4 cells per well in a 24-well plate and starved in serum-free media overnight. Cells were pretreated with wt FTL or AP1-PBNCs (40 nM, 200 nM) at 4 °C for 20 min and then incubated with or without IL-4 (1 nM) for 10 min. After treatment, cells were solubilized in boiling SDS sample buffer, and 10 μg of cell lysates was run with SDS-PAGE. Western blot analyses were performed with anti-STAT6 antibody (#9362; Cell Signaling Technology, Frankfurt, Germany) and antiphospho-STAT6 Ab (#9361; Cell Signaling Technology).

Animals. Wild-type C57BL/6J mice were purchased from Jackson Laboratory (Bar Harbor, ME, USA) and bred in a pathogen-free animal facility. All animals were fed with a normal diet (PMI Lab Diet) *ad libitum* with free access to water. Six- to 8-week-old female mice were used for this study. Animal care and experimental procedures were performed with the approval of the Animal Care Committee of KAIST.

Induction of Experimental Asthma. Asthma induction was performed as previously described.[42] Briefly, *Aspergillus oryzae* protease (1 mg/mL in PBS, Sigma-Aldrich) and chicken egg

ovalbumin (OVA, 0.5 mg/mL in PBS, Sigma-Aldrich) allergens (APO) were mixed 1:9 (v/v) immediately before administration. Mice received four intraperitoneal sensitizations and one final intranasal challenge every 4 days (day 0, 4, 8, 12, 16) with 50 μL of allergen. For intranasal challenge, mice were lightly anesthetized with isoflurane inhalation (Abbott Laboratory, Abbott Park, IL, USA). A 50 μL amount of ^{157}cysAP1-PBNC and wt FTL (1 mg/mL in PBS) was given 1 h before allergen challenge. Low endotoxin of allergen, ^{157}cysAP1-PBNC, and wt FTL was confirmed before administration.

Analysis of Asthma Phenotypes. For phenotypes of allergic asthma, AHR, BAL cytology, BAL glycoprotein assay, and lung histopathology, were determined as described previously.[43] Briefly, 16 h after final intranasal challenge, AHR was measured with a FlexiVent system (SCIREQ Inc., Montreal, Canada). After anesthetization with pentobarbital sodium (Hanlim Pharma Co., Seoul, Korea, 60 mg/kg) and intubation with 20-gauge cannula, mice were connected to the FlexiVent system *via* the endotracheal cannula. After paralyzation with pancuronium bromide (Sigma-Aldrich, 1 mg/kg), mice were ventilated at a respiratory rate of 150 breaths/min and tidal volume of 10 mL/kg against a positive end expiratory pressure of 3 CmH_2O. To measure lung resistances, mice were given incremental doses of methacholine (Sigma-Aldrich) with an inhaler (0 = normal saline only, 1, 3, 9, 18, 27 mg/mL). The airway resistances were allowed to return to the baseline after each dose of methacholine. Then AHR, BAL cytology, and secreted glycoprotein assays were performed as described previously.[44]

Measurement of Secreted Glycoprotein in BAL Fluid. Levels of secreted glycoprotein were measured with modified ELISA as previously reported.[44] Briefly, mucin standard (derived from porcine stomach, Sigma-Aldrich) was diluted 2-fold serially with PBS. BAL fluid samples were also diluted 2-fold serially with PBS beginning at a 1:100 dilution. Each sample (40 μL) was transferred to an ELISA plate (Greiner, Kremsmunster, Austria) and incubated at 37 °C for 2 h. After incubation and washing, plates were blocked with 200 μL of 0.2% I-block (Applied Biosystems, Foster City, CA, USA) and incubated at 37 °C for 2 h. After washing, 40 μL of biotinylated jacalin (5 μg/mL glycoprotein binding lectin, Vector Laboratories, Burlingame, CA, USA) was added and incubated at 4 °C overnight. The next day after another wash, 40 μL of alkaline phosphatase conjugated streptavidin (1:1000 dilution, BD Biosciences) was added, and the plates were incubated at room temperature for 30 min. After a final wash, 70 μL of alkaline phosphatase substrate (5 mmol in 0.1 mol/L alkaline buffer, Sigma-Aldrich) was added and developed until a mucin standard curve was readily apparent. After termination of the reaction with addition of 40 μL of 0.5 N sodium hydroxide, optical density was measured at 405 nm by an ELISA reader (BioRad, Hercules, CA, USA).

Statistical Analysis. Data were presented as mean ± SEM. The nonparametric Mann−Whitney test was used for statistical analysis, and a p value of <0.05 was considered significant. The analyses were performed by using GraphPad Prism software V. 5.0 for Windows (GraphPad Software, La Jolla, CA, USA).

Conflict of Interest: The authors declare no competing financial interest.

Supporting Information Available: A detailed description of the methods followed in this work and additional results are available free of charge *via* the Internet at http://pubs.acs.org.

Acknowledgment. This study was supported by the National Research Foundation of Korea (NRF) grant funded by the Korean government (MEST, 2010-0029206, and MSIP, 2008-0061891); a grant of the Korean Health Technology R&D Project, Ministry for Health & Welfare, Republic of Korea (A121145); and the Kyungpook National University Research Fund, 2012.

REFERENCES AND NOTES

1. Farokhzad, O. C.; Langer, R. Nanomedicine: Developing Smarter Therapeutic and Diagnostic Modalities. *Adv. Drug Delivery Rev.* **2006**, *58*, 1456–1459.
2. Emerich, D. F.; Thanos, C. G. The Pinpoint Promise of Nanoparticle-Based Drug Delivery and Molecular Diagnosis. *Biomol. Eng.* **2006**, *23*, 171–184.
3. Malam, Y.; Loizidou, M.; Seifalian, A. M. Liposomes and Nanoparticles: Nanosized Vehicles for Drug Delivery in Cancer. *Trends Pharmacol. Sci.* **2009**, *30*, 592–599.
4. Torchilin, V. P. Micellar Nanocarriers: Pharmaceutical Perspectives. *Pharm. Res.* **2007**, *24*, 1–16.
5. Brigger, I.; Dubernet, C.; Couvreur, P. Nanoparticles in Cancer Therapy and Diagnosis. *Adv. Drug Delivery Rev.* **2002**, *54*, 631–651.
6. Basarkar, A.; Singh, J. Poly (lactide-co-glycolide)-Polymethacrylate Nanoparticles for Intramuscular Delivery of Plasmid Encoding Interleukin-10 to Prevent Autoimmune Diabetes in Mice. *Pharm. Res.* **2009**, *26*, 72–81.
7. Roy, K.; Mao, H. Q.; Huang, S. K.; Leong, K. W. Oral Gene Delivery with Chitosan--DNA Nanoparticles Generates Immunologic Protection in a Murine Model of Peanut Allergy. *Nat. Med.* **1999**, *5*, 387–391.
8. Furno, F.; Morley, K. S.; Wong, B.; Sharp, B. L.; Arnold, P. L.; Howdle, S. M.; Bayston, R.; Brown, P. D.; Winship, P. D.; Reid, H. J. Silver Nanoparticles and Polymeric Medical Devices: A New Approach to Prevention of Infection?. *J. Antimicrob. Chemother.* **2004**, *54*, 1019–1024.
9. Wilson, D. S.; Dalmasso, G.; Wang, L.; Sitaraman, S. V.; Merlin, D.; Murthy, N. Orally Delivered Thioketal Nanoparticles Loaded with TNF-Alpha-siRNA Target Inflammation and Inhibit Gene Expression in the Intestines. *Nat. Mater.* **2010**, *9*, 923–928.
10. Gupta, A. K.; Gupta, M. Synthesis and Surface Engineering of Iron Oxide Nanoparticles for Biomedical Applications. *Biomaterials* **2005**, *26*, 3995–4021.
11. Pack, D. W.; Hoffman, A. S.; Pun, S.; Stayton, P. S. Design and Development of Polymers for Gene Delivery. *Nat. Rev. Drug Discovery* **2005**, *4*, 581–593.
12. Douglas, T.; Young, M. Viruses: Making Friends with Old Foes. *Science* **2006**, *312*, 873–875.
13. Uchida, M.; Klem, M.; Allen, M.; Suci, P.; Flenniken, M.; Gillitzer, E.; Varpness, Z.; Liepold, L.; Young, M.; Douglas, T. Biological Containers: Protein Cages as Multifunctional Nanoplatforms. *Adv. Mater.* **2007**, *19*, 1025–1042.
14. Flenniken, M. L.; Willits, D. A.; Harmsen, A. L.; Liepold, L. O.; Harmsen, A. G.; Young, M. J.; Douglas, T. Melanoma and Lymphocyte Cell-Specific Targeting Incorporated into a Heat Shock Protein Cage Architecture. *Chem. Biol.* **2006**, *13*, 161–170.
15. Chatterji, A.; Ochoa, W.; Shamieh, L.; Salakian, S. P.; Wong, S. M.; Clinton, G.; Ghosh, P.; Lin, T.; Johnson, J. E. Chemical Conjugation of Heterologous Proteins on the Surface of Cowpea Mosaic Virus. *Bioconjugate Chem.* **2004**, *15*, 807–813.
16. Edwards, C. M.; Cohen, M. A.; Bloom, S. R. Peptides as Drugs. *OJM* **1999**, *92*, 1–4.
17. Kierny, M. R.; Cunningham, T. D.; Kay, B. K. Detection of Biomarkers Using Recombinant Antibodies Coupled to Nanostructured Platforms. *Nano Rev.* **2012**, *3*, 17240http://dx.doi.org/10.3402/nano.v3i0.17240.
18. Lawson, D. M.; Artymiuk, P. J.; Yewdall, S. J.; Smith, J. M.; Livingstone, J. C.; Treffry, A.; Luzzago, A.; Levi, S.; Arosio, P.; Cesareni, G. Solving the Structure of Human H Ferritin by Genetically Engineering Intermolecular Crystal Contacts. *Nature* **1991**, *349*, 541–544.
19. Uchida, M.; Willits, D.; Muller, K.; Willis, A.; Jackiw, L.; Jutila, M.; Young, M.; Porter, A.; Douglas, T. Intracellular Distribution of Macrophage Targeting Ferritin-Iron Oxide Nanocomposite. *Adv. Mater.* **2009**, *21*, 458–462.
20. Valero, E.; Tambalo, S.; Marzola, P.; Ortega-Muñoz, M.; López-Jaramillo, F. J.; Santoyo-González, F.; de Dios López, J.; Delgado, J. J.; Calvino, J. J.; Cuesta, R.; *et al.* Magnetic Nanoparticles-Templated Assembly of Protein Subunits: A New Platform for Carbohydrate-Based MRI Nanoprobes. *J. Am. Chem. Soc.* **2011**, *133*, 4889–4895.
21. Busse, W. W.; Lemanske, R. F. Asthma. *N. Engl. J. Med.* **2001**, *344*, 350–362.
22. Umetsu, D. T.; McIntire, J. J.; Akbari, O.; Macaubas, C.; DeKruyff, R. H. Asthma: An Epidemic of Dysregulated Immunity. *Nat. Immunol.* **2002**, *3*, 715–720.
23. Apter, A. J. Advances in Adult Asthma Diagnosis and Treatment in 2012: Potential Therapeutics and

Gene-Environment Interactions. *J. Allergy Clin. Immunol.* **2013**, *131*, 47–54.
24. Szefler, S. J. Advances in Pediatric Asthma in 2012: Moving Toward Asthma Prevention. *J. Allergy Clin. Immunol.* **2013**, *131*, 36–46.
25. Pelaia, G.; Vatrella, A.; Maselli, R. The Potential of Biologics for the Treatment of Asthma. *Nat. Rev. Drug Discovery* **2012**, *11*, 958–972.
26. Wills-Karp, M. Immunologic Basis of Antigen-Induced Airway Hyperresponsiveness. *Annu. Rev. Immunol.* **1999**, *17*, 255–281.
27. Galli, S. J.; Tsai, M.; Piliponsky, A. M. The Development of Allergic Inflammation. *Nature* **2008**, *454*, 445–454.
28. Nelms, K.; Keegan, A. D.; Zamorano, J.; Ryan, J. J.; Paul, W. E. The IL-4 Receptor: Signaling Mechanisms and Biologic Functions. *Annu. Rev. Immunol.* **1999**, *17*, 701–738.
29. Noben-Trauth, N.; Shultz, L. D.; Brombacher, F.; Urban, J. F.; Gu, H.; Paul, W. E. An Interleukin 4 (IL-4)-Independent Pathway for CD4+ T Cell IL-4 Production is Revealed in IL-4 Receptor-Deficient Mice. *Proc. Natl. Acad. Sci. U.S.A.* **1997**, *94*, 10838–10843.
30. Hong, H. Y.; Lee, H. Y.; Kwak, W.; Yoo, J.; Na, M. H.; So, I. S.; Kwon, T. H.; Park, H. S.; Huh, S.; Oh, G. T.; *et al*. Phage Display Selection of Peptides That Home to Atherosclerotic Plaques: IL-4 Receptor as a Candidate Target in Atherosclerosis. *J. Cell. Mol. Med.* **2008**, *12*, 2003–2014.
31. Montet, X.; Funovics, M.; Montet-Abou, K.; Weissleder, R.; Josephson, L. Multivalent Effects of RGD Peptides Obtained by Nanoparticle Display. *J. Med. Chem.* **2006**, *49*, 6087–6093.
32. Hong, S.; Leroueil, P. R.; Majoros, I. J.; Orr, B. G.; Baker, J. R.; Banaszak Holl, M. M. The Binding Avidity of a Nanoparticle-Based Multivalent Targeted Drug Delivery Platform. *Chem. Biol.* **2007**, *14*, 107–115.
33. Paul, W. E.; Zhu, J. How Are T(H)2-Type Immune Responses Initiated and Amplified?. *Nat. Rev. Immunol.* **2010**, *10*, 225–235.
34. Mathew, A.; MacLean, J. A.; DeHaan, E.; Tager, A. M.; Green, F. H.; Luster, A. D. Signal Transducer and Activator of Transcription 6 Controls Chemokine Production and T Helper Cell Type 2 Cell Trafficking in Allergic Pulmonary Inflammation. *J. Exp. Med.* **2001**, *193*, 1087–1096.
35. Akimoto, T.; Numata, F.; Tamura, M.; Takata, Y.; Higashida, N.; Takashi, T.; Takeda, K.; Akira, S. Abrogation of Bronchial Eosinophilic Inflammation and Airway Hyperreactivity in Signal Transducers and Activators of Transcription (STAT)6-Deficient Mice. *J. Exp. Med.* **1998**, *187*, 1537–1542.
36. Tomkinson, A.; Cieslewicz, G.; Duez, C.; Larson, K. A.; Lee, J. J.; Gelfand, E. W. Temporal Association between Airway Hyperresponsiveness and Airway Eosinophilia in Ovalbumin-Sensitized Mice. *Am. J. Respir. Crit. Care Med.* **2001**, *163*, 721–730.
37. Lee, J. H.; Kaminski, N.; Dolganov, G.; Grunig, G.; Koth, L.; Solomon, C.; Erle, D. J.; Sheppard, D. Interleukin-13 Induces Dramatically Different Transcriptional Programs in Three Human Airway Cell Types. *Am. J. Respir. Cell Mol. Biol.* **2001**, *25*, 474–485.
38. Borish, L. C.; Nelson, H. S.; Lanz, M. J.; Claussen, L.; Whitmore, J. B.; Agosti, J. M.; Garrison, L. Interleukin-4 Receptor in Moderate Atopic Asthma. A Phase I/II Randomized, Placebo-Controlled Trial. *Am. J. Respir. Crit. Care Med.* **1999**, *160*, 1816–1823.
39. Andrews, A. L.; Holloway, J. W.; Holgate, S. T.; Davies, D. E. IL-4 Receptor Alpha Is an Important Modulator of IL-4 and IL-13 Receptor Binding: Implications for the Development of Therapeutic Targets. *J. Immunol.* **2006**, *176*, 7456–7461.
40. Nicholson, G. C.; Kariyawasam, H. H.; Tan, A. J.; Hohlfeld, J. M.; Quinn, D.; Walker, C.; Rodman, D.; Westwick, J.; Jurcevic, S.; Kon, O. M.; *et al*. The Effects of an Anti-IL-13 mAb on Cytokine Levels and Nasal Symptoms Following Nasal Allergen Challenge. *J. Allergy Clin. Immunol.* **2011**, *128*, 800–807 e9.
41. Choi, S.; Choi, K.; Kwon, I.; Ahn, H. The Incorporation of GALA Peptide into a Protein Cage for an Acid-Inducible Molecular Switch. *Biomaterials* **2010**, *31*, 5191–5198.
42. Corry, D. B.; Folkesson, H. G.; Warnock, M. L.; Erle, D. J.; Matthay, M. A.; Wiener-Kronish, J. P.; Locksley, R. M. Interleukin 4, but Not Interleukin 5 or Eosinophils, Is Required in a Murine Model of Acute Airway Hyperreactivity. *J. Exp. Med.* **1996**, *183*, 109–117.
43. Lee, S. H.; Prince, J. E.; Rais, M.; Kheradmand, F.; Shardonofsky, F.; Lu, H.; Beaudet, A. L.; Smith, C. W.; Soong, L.; Corry, D. B. Differential Requirement for CD18 in T-Helper Effector Homing. *Nat. Med.* **2003**, *9*, 1281–1286.
44. Lee, S. H.; Kiss, A.; Xu, J.; Qian, Y.; Bashoura, L.; Kheradmand, F.; Corry, D. B. Airway Glycoprotein Secretion Parallels Production and Predicts Airway Obstruction in Pulmonary Allergy. *J. Allergy Clin. Immunol.* **2004**, *113*, 72–78.